Laser induced fluorescence measurements of the cylindrical Hall thruster plume

R. Spektor,[1] K. D. Diamant,[1] E. J. Beiting,[1] Y. Raitses,[2] and N. J. Fisch[2]
[1]*The Aerospace Corporation, P.O. Box 92957-M2-341, Los Angeles, California 90009-2957, USA*
[2]*Princeton Plasma Physics Laboratory, P.O. Box 451, Princeton, New Jersey 08543-0451, USA*

(Received 1 April 2010; accepted 15 July 2010; published online 17 September 2010)

An investigation of a fully cylindrical Hall thruster was performed using laser induced fluorescence (LIF) to measure ion velocity profiles in the plume. The measurements confirm a previously reported 9% increase in the exhaust energy when the cathode keeper draws an excess current (overrun mode). Furthermore, the velocity directions in the plume remain relatively unchanged for the cusped and direct magnetic field configuration in both overrun and nonoverrun modes. Previously reported plume narrowing in the overrun mode was confirmed and found to be due to the shift of the acceleration and ionization regions toward the anode. The electric field inferred from the LIF measurements allowed calculation of the electron $E \times B$ drift. Close to the centerline of the thruster, electrons drift azimuthally with velocity decreasing away from the centerline, thus creating shear. This shear can be a source of plasma instabilities and influence electron transport. Further away from the centerline, electrons drift in the opposite direction with their velocity increasing with increasing radius. In that region, electrons rotate without shear. © *2010 American Institute of Physics*. [doi:10.1063/1.3475433]

I. INTRODUCTION

Hall thrusters are not easily amendable to miniaturization. A number of methodologies are available for scaling the thrusters to power levels below a few hundred watts while attempting to preserve specific impulse and efficiency.[1–6] Raitses *et al.*[7] developed a cylindrical Hall thruster (CHT) that operates around 200 W, featuring a reduced surface-to-volume ratio and unique magnetic topology. The central magnetic pole and inner ceramic of the CHT are shortened to produce an annular region near the anode, which is followed by a cylindrical region. Electrons are confined in the annular region by the mainly radial magnetic field, as in conventional annular Hall thrusters. The magnetic field in the cylindrical region has both a substantial axial component and a large axial gradient. Electron trapping in that region occurs by magnetic mirroring near the annular part of the channel and by the adverse potential gradient on the cathode side.[8] Ion acceleration occurs mainly in the low surface-to-volume cylindrical region resulting in reduced particle losses.[8–10]

The CHT exhibits low discharge current oscillations[9] and high ionization efficiency,[11] comparable to a conventional Hall thruster. For normal thruster operation the plume divergence is large, but by "overrunning" the discharge current in 2.6 and 3 cm diameter CHTs, the divergence is reduced by 20%–30% (from 71° to 53°). The ion energy distribution is also shifted to higher energies with the primary ion peak energies increased by 9% and fewer primary ions at high angles.[12,13] The overrun regime is attained by running a current to the keeper of the hollow cathode during normal operation. Anode efficiencies of 33%–41% (not including power required to overrun the discharge) at 50–175 W were measured with the 2.6 cm thruster.[12] Very similar results[13] were obtained when the CHT was modified to remove the annular region (i.e., the inner channel wall ends flush with the anode downstream face), producing a fully cylindrical Hall thruster (FCHT), as shown in Fig. 1.

The underlying physical processes responsible for the enhanced performance in the overrun regime are not fully understood. Recent probe measurements showed that the potential drop inside the channel increases in the overrun regime.[14,15] It was suggested that this also contributes to the plume narrowing. In this paper we use laser induced fluorescence (LIF) to investigate these reported improvements through a series of comparisons between the ion velocity distributions in various thruster operating regimes. Specifically, we focus our attention on the FCHT configuration and study the differences between the overrun and the nonoverrun modes with two magnetic field topologies. We use the LIF technique to map ion velocities in the plume and infer electric fields for all four permutations of magnetic fields and current overrun regimes. The rest of the paper is organized as follows. The setup of the LIF apparatus is described in the next section. Then we present the experimental results and discuss our findings. We conclude with some final remarks and suggestions for future work.

II. EXPERIMENTAL SETUP

The experiments were performed in the Near Field Facility (NFF) at The Aerospace Corporation. The facility comprises a 3 m long and 1.5 m diameter stainless steel chamber pumped by two He-cooled nude sails with the speed of 42 000 l/s on Xe. The system is capable of maintaining a base pressure of 5×10^{-7} Torr; this increases to as much as 7×10^{-6} Torr (adjusted for Xe) with a thruster operating. All pressures were measured with an ionization gauge mounted on the side of the chamber at the same axial location as the thruster. A detailed description of the NFF chamber is given in Ref. 16.

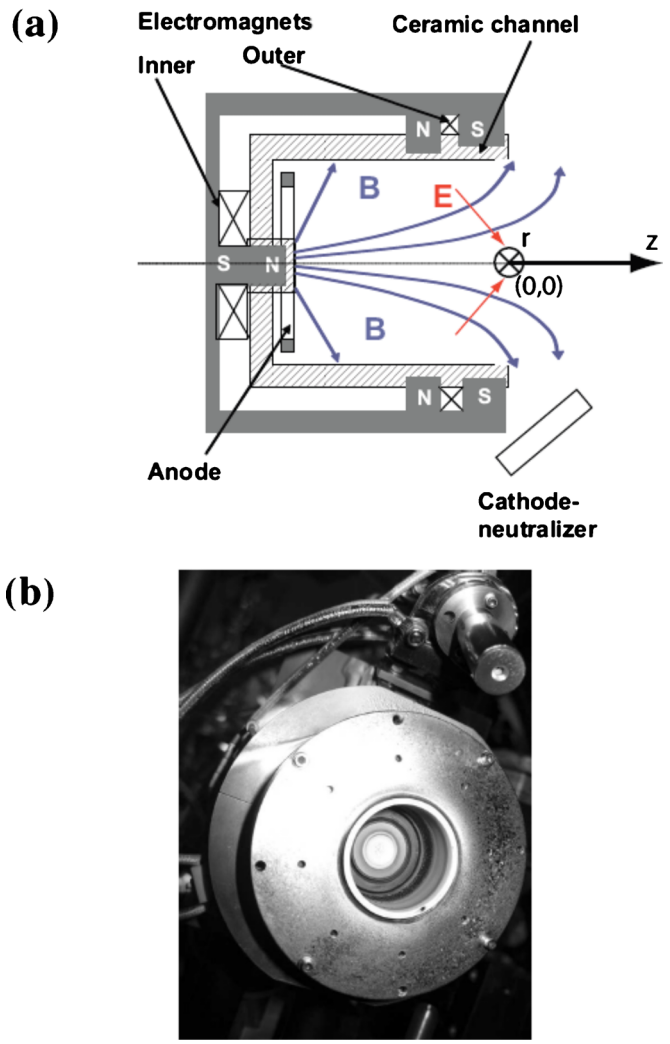

FIG. 1. (Color online) Panel (a) schematic of the FCHT thruster operated in the direct configuration and panel (b) a picture of the FCHT with the HWPES-250 cathode. The FCHT thruster is a modified CHT without the annular region.

The FCHT consists of a boron-nitride ceramic channel, an annular anode, which also acts as the gas distributor, two electromagnet coils, and a magnetic core. The channel is 3 cm in diameter and the thruster exit is located 2.2 cm from the anode. The magnet coils can be run in either a direct configuration, which produces an enhanced axial component of the magnetic field at the outer wall and a stronger magnetic mirror on the thruster axis[17,18] or in the cusped configuration, which produces enhanced radial component of the magnetic field. In the cusped configuration, the inner and outer magnet poles have the same polarity sense, and in the direct configuration, shown in Fig. 1(a), the outer magnet polarity is reversed. A commercial hollow cathode (Heatwave Laboratories model HWPES-250) supplies electrons to the discharge and plume. The cathode keeper exit aperture is located 5.4 cm radially from thruster centerline, and 2.0 cm downstream of the thruster exit plane. The angle between the thruster and cathode axes is approximately 40°. A photograph of the thruster is shown in Fig. 1(b).

For the experiments described here, we operated the thruster with the discharge voltage of 250 V and current near 0.6 A. Magnet coil current magnitudes were 2 A (inner) and 1.5 A (outer) in both direct and cusped configurations. The keeper drew 3 A in the overrun mode and was off for non-overrun operation. The flow rate was 4 and 2 SCCM (SCCM denotes cubic centimeter per minute at STP) for the anode and cathode, respectively.

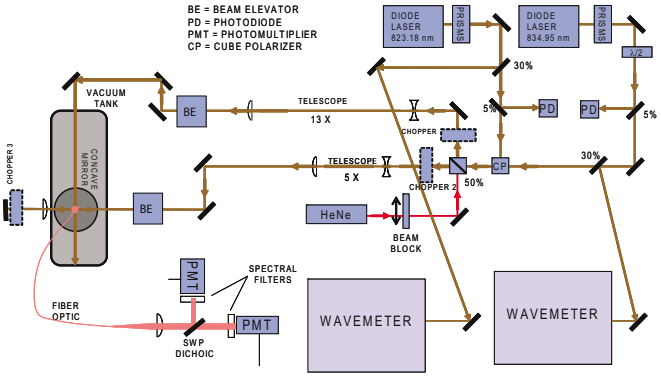

FIG. 2. (Color online) Schematic of the LIF setup used for the FCHT measurements.

The thruster was placed on a motorized platform that could be translated in three orthogonal directions; its exhaust was directed toward the helium-cooled sails. This platform allowed us to perform spatially resolved measurements in the plume by moving the thruster relative to a stationary collection optics and the LIF apparatus. The data were collected in steps of 0.5 cm in the region spanning from the thruster exit to 4.0 cm along the z direction, and from the thruster centerline to 3.0 cm along the radial direction, with the thruster exit at the centerline defined as the origin, as shown in Fig. 1(a).

The LIF instrument shown in Fig. 2 is designed to measure two-dimensional velocity distribution function profiles of Xe ion and neutral species simultaneously. It is an expanded version of the apparatus previously used to investigate the SPT-140 thruster.[19,20] While similar in operation to LIF methods used by other authors,[21–23] our arrangement has some unique features, which are described below. For this work we used only the Xe^+ portion of the setup. A TLB-6000 series New Focus tunable diode laser with the center vacuum wavelength of 834.95 nm (driven by a Vortex controller) excited the $5d^4F_{5/2}-6p^4D_{5/2}$ transition in Xe^+. The laser is able to provide up to 17 mW of power and maintain mode-hop free operation over a range of 60 GHz. The laser beam was divided into two components, each of which was sent through a series of mirrors and a telescope to cross orthogonally in the NFF vacuum chamber. One beam entered the end of the chamber and measured the axial component of ion velocity; the other entered the side and measured the transverse component of ion velocity. The transverse and axial beam powers were 1.5 and 1 mW, respectively. The transverse beam was reflected from an external mirror and refocused onto the crossing point of the transverse and axial beams. These forward and reflected transverse signals provided a reliable zero-velocity reference, which was also verified by the wavemeter reading. The absence of the LIF signal saturation was verified up to the maximum laser power. The

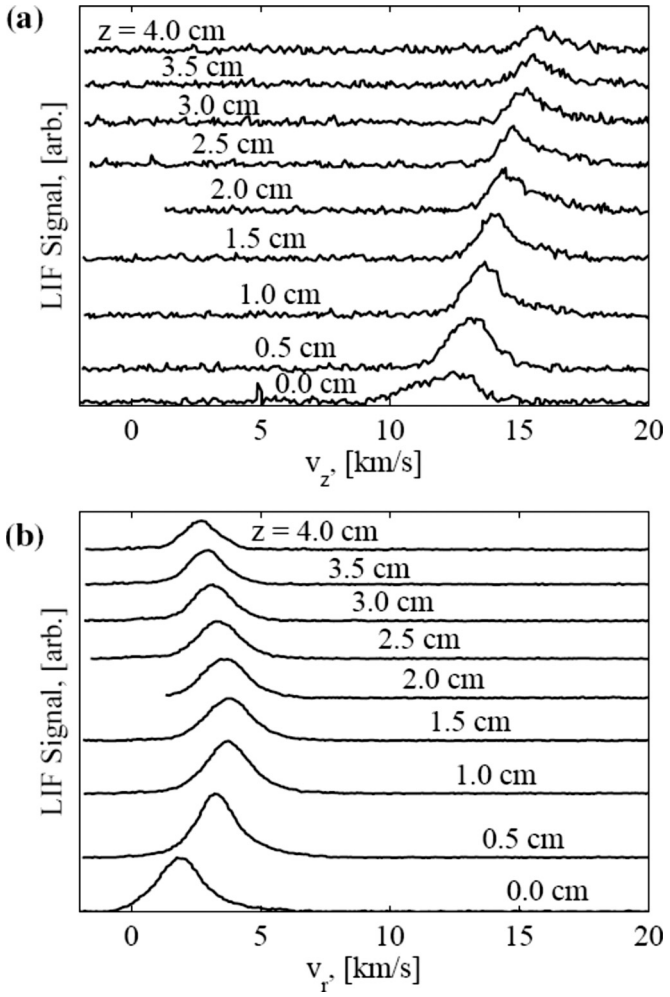

FIG. 3. Evolution of Xe^+ velocity distribution as a function of distance from the thruster exit at $r=1$ cm. The thruster was operated in the direct configuration in the overrun mode. Panel (a) shows the axial velocity component and panel (b) shows the transverse velocity component.

three beams were optically chopped at different frequencies. He–Ne and green diode lasers (not shown in Fig. 2) aided alignment.

The LIF signal from the $6p^4D_{5/2}-6s^4P_{3/2}Xe^+$ transition at 542 nm was collected by a 15 cm concave mirror and focused onto a 2 mm diameter fiber optic bundle, as described in Ref. 16. A lens installed near the fiber optic bundle improved the signal-to-noise ratio by optimizing the focal point size for the laser beam waist. The light exiting the fiber optic bundle passed through a 10 nm bandwidth interference filter and was focused on a photomultiplier tube (PMT). The electrical signal from the PMT was divided among three Stanford Research SR830 lock-in amplifiers, each tuned to one of the three chopper frequencies. A Burleigh WA-1500 wavemeter measured the laser wavelength during the laser sweeps.

Each data set consisted of a 300 data point scan and typically covered a frequency range of 40 GHz. Figure 3 displays scans of the axial (panel a) and transverse (panel b) ion velocity distributions at various axial positions and $r=1$ cm with the thruster running in the overrun mode and the magnetic coils in the direct configuration. Each trace in Fig. 3 consists of a single scan. At a few locations where the LIF signal-to-noise ratio was low, we collected up to three scans to reduce the measurement uncertainty. The plots in Fig. 3 show that the LIF signal was clean with low noise.

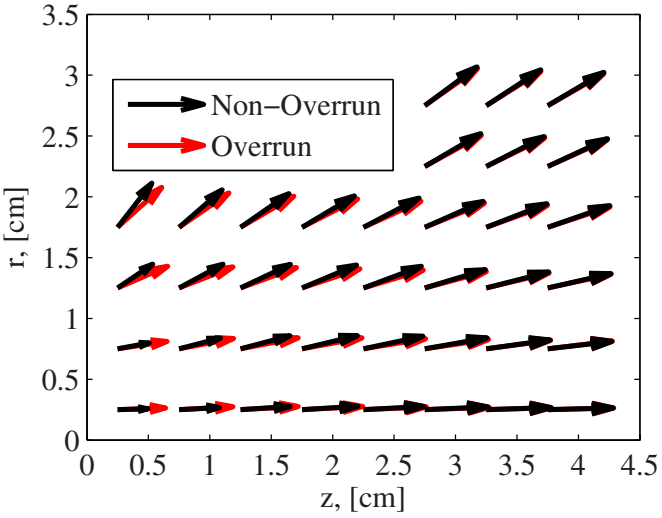

FIG. 4. (Color online) Ion velocity vector maps in the plume of the FCHT thruster in the direct configuration. The nonoverrun case is shown by the black arrows, while the overrun case is shown by red (gray) arrows.

III. RESULTS AND DISCUSSION

Figure 4 shows a two-dimensional ion velocity vector map, which we obtained from the LIF measurements with the thruster running in the direct magnetic field configuration. The thruster exit was located at $z=0$ cm with the thrust axis pointing along the z direction. The channel lip was located at $r=1.5$ cm with the thruster centerline at $r=0$ cm. Velocity vectors were determined from the first moment of the velocity distribution. The black arrows designate the nonoverrun configuration while the red arrows correspond to the overrun regime of operation. Velocity divergences for the overrun and nonoverrun cases shown in the figure are very similar. Furthermore, the figure shows that velocity vectors are directed along the z axis in the regions close to the centerline. Away from the centerline, velocity divergence increases. The velocity vector maps for the cusped magnetic field configuration in both overrun and nonoverrun modes look very similar to the maps shown in Fig. 4.

The quantitative differences between the overrun and nonoverrun velocities are hard to discern from the vector map of Fig. 4. To demonstrate some of these differences, we plot the axial component of ion velocity along the thruster centerline for the overrun and nonoverrun cases with both magnetic field profiles in Fig. 5(a). In both cusped and direct configurations, the overrun LIF data show ~7% increase in the ultimate exhaust velocity (v_z at $z=4$ cm) over the corresponding nonoverrun cases. Similar findings from the probe measurements have been reported for the direct magnetic field configuration in Ref. 13. Figure 5(b) shows the centerline potential profiles corresponding to modes shown in Fig. 5(a). Here we have arbitrarily assigned zero volt potential at

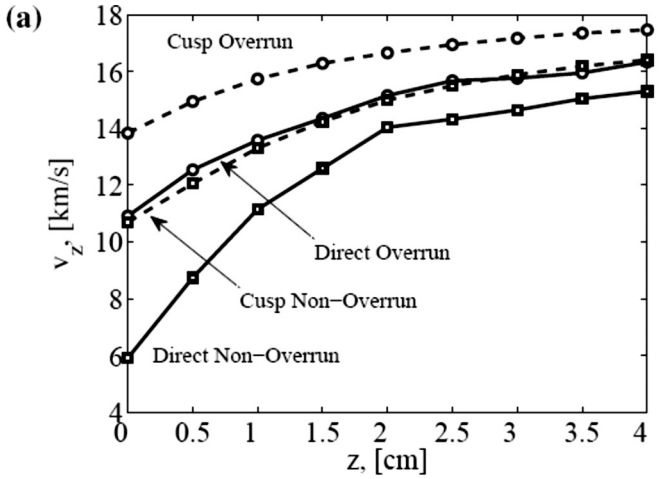

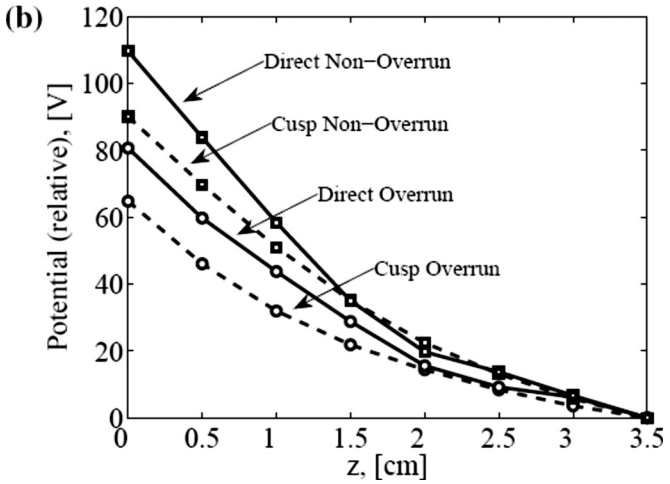

FIG. 5. Panel (a) shows centerline velocity profiles for the four studied regimes. Solid lines represent direct magnet configuration, while dashed lines represent cusped configuration. Squares designate the nonoverrun condition, while circles designate the overrun cases. Panel (b) shows relative potential profiles along the centerline in the FCHT plume for the same four modes shown in panel (a). $U=0$ V was arbitrarily assigned at $z=3.5$ cm for all for modes.

$z=3.5$ cm for all thruster regimes. This is a reasonable assumption since ion velocities plateau near that point.

In the nonoverrun mode with the direct magnetic field configuration, the ion velocity at the thruster exit is 6 km/s while the ultimate exhaust velocity is 14 km/s. Thus, more than half of the acceleration in this regime occurs in the thruster plume. We contrast this with the overrun mode with the cusped magnetic field configuration, where most of the acceleration occurs inside the thruster. Figure 5(a) shows that for both magnetic field configurations, the acceleration region in the overrun mode is located closer to the anode than in the nonoverrun mode. This observation supports recently published probe measurements of plasma potential profiles[15] and may result from changes in electron mobility at the channel exit.

The shift of the acceleration region toward the anode in the overrun mode also corresponds to narrowing of the plume.[12,13] It is interesting to note, however, that there is no significant change in velocity divergence between the overrun and nonoverrun modes, as shown in Fig. 4. The observed plume narrowing can thus be attributed to an increase in plasma density close to the centerline, as reported in Ref. 13.

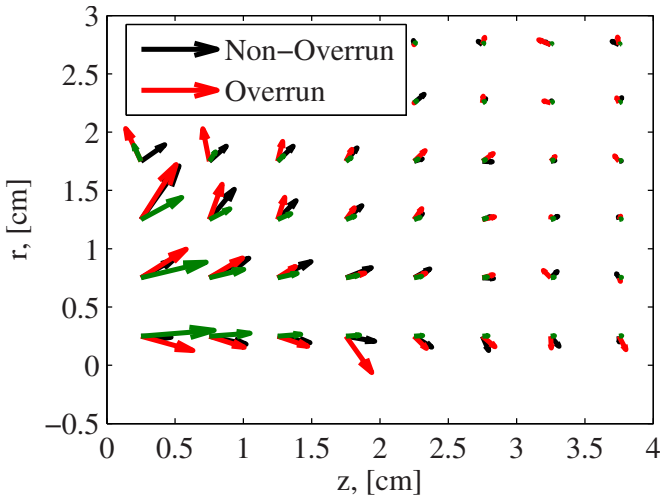

FIG. 6. (Color online) Measured magnetic and calculated electric field profiles in the plume of the FCHT thruster. Green arrows (dark gray) designate magnetic field vectors. Red arrows (lighter gray) designate electric field vectors in the overrun regime and black arrows show the non-overrun mode.

The larger ultimate ion velocity in the overrun case indicates that not only does the acceleration region move inward, as shown by the potential profiles in Fig. 5(b), but the ionization region also moves toward the anode. For example, calculating the total potential fall for the direct configuration, we see that in the overrun case the ions are born at a potential, which is ~20 V above the nonoverrun case. Recent RPA (Retarding Potential Analyzer) measurements further support that conclusion,[12] showing that in the overrun regime the peak of the ion energy distribution shifts to higher values.

The two-dimensional (2D) LIF ion velocity distribution measurements also allow us to calculate the electric field profile in the plume of the FCHT. Here we present the electric field obtained by taking moments of the Boltzmann equation with the measured ion velocity distribution functions.[24] That method is an extension of one-dimensional method derived by Pérez-Luna *et al.*[25] The method presented in Ref. 24 can be applied to a 2D velocity distribution that is separable into its axial components, i.e., $f(v_x,v_y)=l(v_x)g(v_y)$. Figure 3 shows that most LIF traces resemble the Maxwellian distribution, which is separable. A simplified analysis involving the ion fluid conservation equation has been previously described in Ref. 26. We should note that the electric field presented here differs significantly in some regions of the plume from the field shown in Ref. 26. In particular, in the region close to the centerline of the thruster, where the ion pressure tensor contribution is not negligible, the current method provides a better estimation of the field. Away from the centerline, the two results produce similar answers. We should also note that the obtained electric field is a time-averaged quantity since the LIF measurements were performed on a time scale which is much longer that a typical plasma oscillation period.

Figure 6 shows the 2D electric field vector maps for both

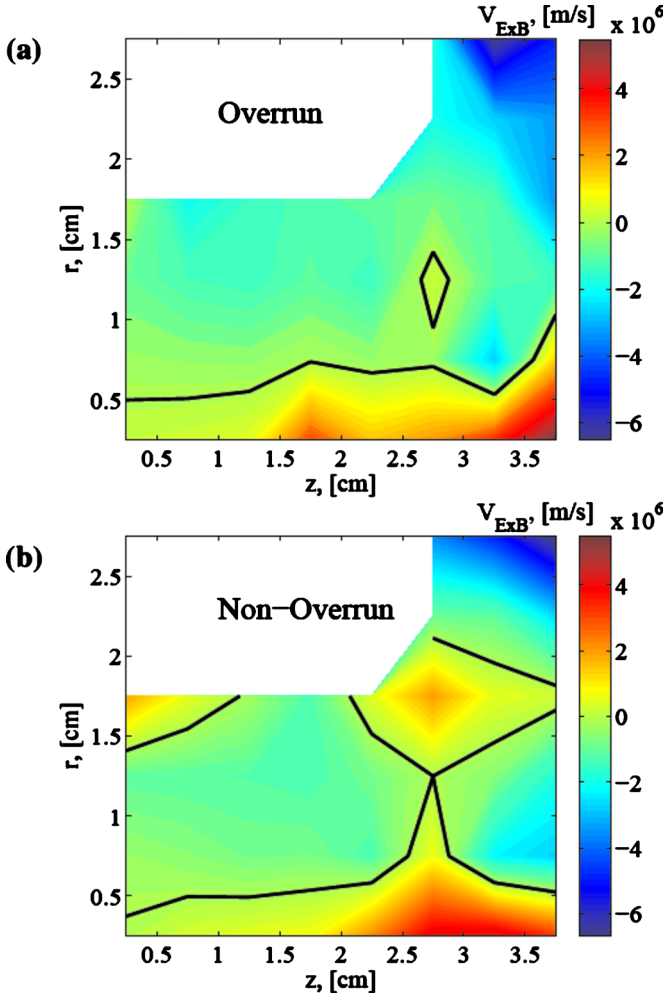

FIG. 7. (Color online) The $E\times B$ electron velocity in the plume of the FCHT thruster. Panel (a) shows the overrun case while panel (b) shows the nonoverrun case. The white area in the upper left corner of each panel corresponds to the region where the LIF measurements were unreliable. The black lines correspond to zero $E\times B$ velocity and separate the regions of positive and negative rotation.

overrun and nonoverrun regimes in the direct magnetic field configuration. Once again, the black arrows correspond to the nonoverrun mode, while the red arrows correspond to the overrun mode. The cusp profiles, which are not shown, look very similar. The measured (with the thruster off) magnetic field is shown by green arrows. The shallow angle between the electric and magnetic field vectors indicates that the magnetic field lines are not equipotential in the plume. Furthermore, close to the centerline the radial component of the electric field is negative, while further away the field points away from the centerline. This reversal in the radial component direction is not caused by the pressure gradient, which points away from the centerline in the FCHT.[13]

With the measured electric and magnetic fields, we can also compute the $E\times B$ electron velocity in the plume. This velocity is depicted in Fig. 7 for the overrun and nonoverrun cases. Within the shown range, the Larmor radius does not exceed 1 cm. The white region in the upper left corner of each panel corresponds to locations where LIF measurements could not be obtained. We notice that in general for both overrun and nonoverrun cases, the $E\times B$ velocity tends to increase away from the thruster exit. The $E\times B$ velocity, which is proportional to $E/B\cdot\sin\theta$, increases either because the B-field decreases faster than E-field or angle θ increases.

We observe two very different regions of the electron $E\times B$ drift. In the region close to the centerline of the thruster, the electrons drift in the positive direction. In the region further away from the centerline, electrons drift in the negative direction. The black lines in Fig. 7 separate these two regions. In the region close to the centerline, the positive velocity decreases with the radial distance creating shear and leading to plasma instabilities, which in turn can influence electron transport. In the region away from the centerline, the negative velocity increases with the radial distance producing an isorotating plasma (rotating without shear). It is prudent to note that the electric field calculations require taking second derivatives of the velocity moments. Coupled with the coarse spatial distribution of the data points (0.5 cm), this can lead to a large error in the electric field and the $E\times B$ estimation. Thus, the maps shown in Fig. 7 should be viewed as a qualitative guide of the electron motion rather than the absolute measurements.

Calculating the electron thermal speed with $T_e\approx 5$ eV, we find that a large portion of electrons drifts at supersonic speeds. This electron drift induces an axial magnetic field ($\sim$0.01 G) that is orders of magnitude smaller than the applied field ($\sim$100 G). Finally, we note that two other drift components may exist in the plasma besides the $E\times B$ drift. The ∇B drift and diamagnetic current components can provide significant contribution to the Hall current. In our case we estimate each of these components to be small—on the order of 10^4 m/s, which is two orders of magnitude smaller than a typical $E\times B$ velocity.

IV. CONCLUSIONS

In this paper we reported on the Xe^+ LIF measurements in the plume of the FCHT thruster. The measurements were performed with the thruster operating in the overrun and nonoverrun modes as well as with magnetic field in the direct and cusped configurations. We found that the ultimate exhaust velocity increases by approximately 7% in the overrun regime for both magnetic field configurations. The overrun regime in the cusped magnetic field configuration resulted in the highest ultimate exhaust velocity (17 km/s) of the four modes that we studied. Surprisingly, velocity vector map showed that there is very little difference in the ion velocity direction in the plume between all four modes. This result suggested that the observed plume narrowing in the overrun mode is due to the shift in the location of the ionization and acceleration regions toward the anode and an increased ion production closer to the centerline. However, nonzero radial component of ion velocity distribution allows contributions from other regions of the thruster. These conclusions support previous invasive probe measurements made inside the thruster.[15] Potential profiles extracted from the velocity measurements indicated that in the overrun regime a larger portion of the potential fall occurred inside the thruster.

We also found that the magnetic field lines outside the thruster are not equipotential. Using the calculated electric and measured magnetic fields, we computed the $E \times B$ electron velocity. We found that two distinct regions of the $E \times B$ drift exist in the plume of the FCHT. In one region, which is close to the centerline of the thruster, electrons drift velocity decreases toward zero with increasing radius, thus creating strong shear. Shear can cause plasma instabilities and influence electron transport. Further away from the centerline, the electrons drift in the opposite direction. In that region, the electron velocity increases with increasing radius. Our calculations showed that in this region electrons isorotate at a velocity higher than the electron thermal speed. The low plasma density in the region however, ensures that the magnetic field induced by this drift is negligible when compared to the applied field.

ACKNOWLEDGMENTS

The authors thank Dr. Artem Smirnov for fruitful discussions. The project was supported by The Aerospace Corporation through its Independent Research and Development Program.

[1] V. Khayms and M. Martinez-Sanchez, *Proceedings of the 32nd Joint Propulsion Conference*, Lake Buena Vista, FL, 1996 (American Institute of Aeronautics and Astronautics, Washington D.C., 1996).
[2] V. Hruby, J. Monheiser, B. Pote, P. Rostler, J. Kolencik, and C. Freeman, *Proceedings of the 30th Plasmadynamics and Lasers Conference*, Norfolk, VA, June 1999 (American Institute of Aeronautics and Astronautics, Washington D.C., 1999).
[3] N. Z. Warner and M. Martinez-Sanchez, *Proceedings of the 42nd Joint Propulsion Conference*, Sacramento, CA, 2006 (American Institute of Aeronautics and Astronautics, Washington D.C., 2006).
[4] F. Battista, E. DeMarco, T. Misuri, and M. Andrenucci, *Proceedings of the 30th International Electric Propulsion Conference*, Florence, Italy, 2007, IEPC-2007–313 (Electric Rocket Propulsion Society, Fairview Park, 2007).
[5] M. Belikov, O. Gorshkov, E. Dyshlyuk, A. Lovtzov, and A. Shagayda, *Proceedings of the 30th International Electric Propulsion Conference*, Florence, Italy, 2007 (Electric Rocket Propulsion Society, Fairview Park, 2007).
[6] E. Ahedo and J. Gallardo, *Proceedings of the 28th International Electric Propulsion Conference*, Toulouse, France, 2003 (Electric Rocket Propulsion Society, Fairview Park, 2003).
[7] Y. Raitses, N. J. Fisch, K. M. Ertmer, and C. A. Burlingame, *Proceedings of the 36th Joint Propulsion Conference*, Huntsville, AL, 2000 (American Institute of Aeronautics and Astronautics, Washington D.C., 2000).
[8] A. Smirnov, Y. Raitses, and N. J. Fisch, Phys. Plasmas **14**, 057106 (2007).
[9] Y. Raitses and N. J. Fisch, Phys. Plasmas **8**, 2579 (2001).
[10] A. Smirnov, Y. Raitses, and N. J. Fisch, J. Appl. Phys. **95**, 2283 (2004).
[11] A. Smirnov, Y. Raitses, and N. J. Fisch, J. Appl. Phys. **94**, 852 (2003).
[12] Y. Raitses, A. Smirnov, and N. J. Fisch, Appl. Phys. Lett. **90**, 221502 (2007).
[13] K. D. Diamant, J. E. Pollard, Y. Raitses, and N. J. Fisch, IEEE Trans. Plasma Sci. **38**, 1052 (2010).
[14] E. M. Granstedt, Y. Raitses, and N. J. Fisch, J. Appl. Phys. **104**, 103302 (2008).
[15] Y. Raitses, A. Smirnov, and N. J. Fisch, Phys. Plasmas **16**, 057106 (2009).
[16] R. Spektor and E. J. Beiting, *Proceedings of the 30th International Electric Propulsion Conference*, Florence, Italy, 2007 (Electric Rocket Propulsion Society, Fairview Park, 2007).
[17] A. Smirnov, Y. Raitses, and N. J. Fisch, *Proceedings of the 29th International Electric Propulsion Conference*, Princeton, NJ, 2005 (Electric Rocket Propulsion Society, Fairview Park, 2005).
[18] A. Smirnov, Y. Raitses, and N. J. Fisch, IEEE Trans. Plasma Sci. **34**, 132 (2006).
[19] E. J. Beiting and J. E. Pollard, Proceedings of the Third International Conference of Spacecraft Propulsion, Cannes, France, 2000.
[20] J. E. Pollard and E. J. Beiting, Proceedings of the Third International Conference of Spacecraft Propulsion, Cannes, France, 2000.
[21] W. A. Hargus, Jr. and M. A. Cappelli, J. Propul. Power **18**, 159 (2002).
[22] W. A. Hargus and M. R. Nakles, *Proceedings of the 42nd Joint Propulsion Conference*, Sacramento, CA, 2006 (American Institute of Aeronautics and Astronautics, Washington D.C., 2006).
[23] S. Mazouffre, V. Kulaev, and J. Pérez-Luna, Plasma Sources Sci. Technol. **18**, 034022 (2009).
[24] R. Spektor, Phys. Plasmas **17**, 093503 (2010).
[25] J. Pérez-Luna, G. J. M. Hagelaar, L. Garrigues, and J. P. Boeuf, Plasma Sources Sci. Technol. **18**, 034008 (2009).
[26] R. Spektor, K. D. Diamant, E. J. Beiting, Y. Raitses, and N. J. Fisch, *Proceedings of the 31st International Electric Propulsion Conference*, Ann Arbor, MI, 2009 (Electric Rocket Propulsion Society, Fairview Park, 2009).